Exploring Biological Samples in 3D Beyond Classic Electron Tomography

Marcel Cunha, Cédric Messaoudi and Sergio Marco

Institut Curie, Centre de Recherche and INSERM

Developments of electron tomography methods are of great importance to unravel the tridimensional organization and the interior detail of objects of nanometric scale. Here we describe two recently developed approaches to surpass some of the milestones of contemporary electron tomography: The low signal to noise ratio of tomograms and the detection of chemical elements in 3D. The techniques applied rely on STEM tomography and EFTEM tomography, capabilities of the 200kV electron microscope JEOL JEM-2200FS equipped with an in-column energy filter and STEM detectors. In the resin embedded samples tested, STEM-HAADF tomography was applied with success to improve the signal to noise ratio and determine cytoskeletal structures on mammalian kidney cells (LLC-PK1). For elemental detection, EFTEM tomography revealed the precise location and 3D arrangement of iron particles bound to cell wall of the pathogenic fungus ***Fonsecaea pedrosoi***. Both techniques resulted in datasets clear enough for direct interpretation and threshold-based segmentation.

Introduction

Imaging techniques of tridimensional reconstructions provide details of the interior of reconstructed objects otherwise inaccessible. Such methods allow the quantification of volumes and might give access to the information of the different elements constituting the object. They are used in many fields such as archeology, geophysics, material sciences, quality control and biology. In medicine, these methods represented by X-ray tomography [1], single photon emission computed tomography [2], magnetic resonance imaging [3] or positron emission tomography [4] are regularly used for exploration and diagnosis. In cell biology, volume reconstruction methods provide a more accurate vision of the relationships between cellular structures and organelles leading to a better understanding of life processes [5]. Thus, methods to obtain 3D information of objects are nowadays indispensable for large aspects of modern science.

3D reconstruction methods are usually based on the stacking of images obtained from sections of the studied object or on the combination of data from its projections. The electron microscopy techniques available nowadays which use the first approach are destructive to the specimen, since they are based on the progressive slicing by knives or by sample erosion by an ion beam. The second approach, used for electron tomography, is based on the analysis of the projections of a thick specimen (from 100 to 1000 nanometers), which is preserved and could be used for successive and complementary analyses. This is one reason that makes approaches based on reconstruction techniques from projections largely favored. These methods require image formation by the use of any kind of penetrating wave generated by a tomograph which also records the projected images [6]. To study samples at nanometric scale, the transmission electron microscope (TEM) is presently the most used tomograph although other alternatives are slowly being applied to life sciences, such as those based on synchrotron radiation [7]. Volume reconstructions methods based on the combination of TEM images acquired from a single specimen tilted at different angles are called transmission electron tomography (TET) [8]. The automation of image acquisition using TEMs started a quarter of century ago and was perfected more recently with the use of fast computers and sensitive and larger digital cameras sensors. This enabled TET as a routine in a reasonable number of well-equipped electron microscopy laboratories. In biology, TET has recently been combined with cryo-fixation methods [9,10] consisting in the freezing of samples at speed, pressure and temperature conditions to reach a quality of ice

U759 Orsay, F-91405 France

sergio.marco@curie.fr

known as the vitreous state of the water. Since cells are mainly composed by water, its non-crystaline vitreous state formation by cryo-fixation allows a preservation of cellular structures in a close-to-native state. Cryo-fixation can then be followed by a replacement of water for resins (cryo-substitution) or by direct observation of the sample into the electron microscope at liquid nitrogen or lower temperatures (cryo-electron microscopy and cryo-electron tomography when combined with electron tomography). Cryo-electron tomography (CET) [11] is one of the most informative 3D approaches in structural cell biology, despite its limitations on sample size and resolution, which is approximately 5 nm for most used TET conditions, is currently becoming more and more popular among biologists, but it is still far from being widely used in biology labs.

In parallel to the development of CET, other electron tomographic approaches, valid for both resin embedded biological specimens and material sciences samples, are in progress. For this, the two main challenges are: (I) to increase the quality (resolution and signal-to-noise ratio) of the 3D reconstructions; and (II) to get 3D chemical distribution of elements. The first is considerably important to define small cellular structures like cytoskeletal filaments and other protein-made supramolecular structures and its subunits without the need to isolate such from the cellular environment. The latter is becoming increasingly interesting for biologist to help to unravel the role of elements (e.g. Iron, phosphorous) related to its location in the cell and its association with other cellular structures or organelles.

The improvement of the TET approaches in resin embedded samples goes presently through its combination with Scanning Transmission Electron Microscopy in its different modes (STEM-BF, ADF or HAADF) [12] allowing the enhancement of the signal-to-noise ratio of the projections; and also through its combination with Energy filtered TEM (EFTEM) to go further than the structural information by obtaining 3D chemical maps. STEM and EFTEM are frequently used in material sciences [13] but they are less common in the study of biological specimens. In this manuscript, we illustrate the potential that combining these two imaging modes with electron tomography has in biology by two examples consisting in the visualization of cytoskeleton elements in mammalian cells and the iron localization around a fungal cell wall.

The cytoskeleton [14] is not only the cellular scaffold, but also plays essential roles in a series of cellular phenomena like cellular division, cell growth, movement and intracellular transport of organelles. In eukaryotic cells, the cytoskeleton contains three main kinds of filaments: (I) actin filaments, constituted by double helix of 7 nm of diameter; (II) intermediate filaments, having about 10 nm of diameter; and (III) microtubules, which are cylinders of about 25 nm diameter. A high number of contemporary questions regarding the above cited phenomena are related to the precise determination of cytoskeleton structures in cell and the relation of its tridimensional structure with nearby organelles or associated proteins.

Cellular structures are not only related to the cellular constitution and maintenance but also to interaction with other cells, from the same or other organism. The interaction between different organisms may result in growth of one in detriment of the other designing infection. The virulence of pathogenic fungi depends on several factors, and an important one is the presence of a pigment named melanin, mostly located on the fungal cell wall, providing strength and shape to the cell and related to resistance of antifungal treatments [15,16]. Since melanin interacts with iron forms, its spatial localization can be tackled by studying the 3D distribution of iron exogenously added via cationized ferritin. This requires the computation of 3D maps of iron by EFTEM tomography (EFTET).

Experimental, Results and Discussion, etc.

Data acquisition and image analysis

Images were acquired on a JEOL JEM-2200FS equipped with an in-column energy filter and a ssCCD 2k × 2k Gatan camera. For standard TET, Z-loss tilted series were acquired using an energy window of 10 eV. In the case of STEM-HAADF tomography images were recorded via JEOL's TEMography software suite for STEM. For EFTEM tomography tilt series at 0, 20, 560, 590, 620, 650, 680 and 710 eV were acquired also with JEOL's acquisition software suite. Image alignment was performed using Etomo [17,18] and TomoJ [19,20] depending on the addition or not of fiducial markers (5nm gold beads). 3D reconstructions were performed in Etomo or TomoJ using WBP or ART algorithms respectively both using a GPU accelerated implementation. For EFTET, background subtraction and image reconstruction were performed after multivariate analysis using an ImageJ plug-in developed by our group (unpublished software).

Comparison between standard TET and STEM-HAADF tomography

Brush border microvilli cells derived from proximal tubule of porcine kidney epithelium (LLC-PK1) were used for visualization of cytoskeleton elements by STEM and STET. A standard procedure consisting to fix samples with phalloidin and aldehydes, post-fix with tannic acid and osmium (TOTO), dehydrate and embedding in epon resin was applied before obtaining 100 nm thick sections.

Since contrast in STEM-HAADF is directly related to the atomic number of the elements present in the sample (Z-contrast image), this imaging mode is able to produce data presenting higher signal-to-noise ratio than standard TEM in stained biological samples (**Figure 1**A,B). However, in most of 2D studies performed in stained biological samples, the SNR improvement does not justify the use of STEM. For instance, in our data set, different components of the cytoskeleton such as microtubules or actin could be identified in both cases. In addition, for an equivalent surface, the acquisition time required to record STEM images is larger than that required in standard TEM mode. Nevertheless, the SNR enhancement that can be achieved by STEM-HAADF is useful to improve 3D reconstructions computed by electron tomography because it improves image alignment (without fiducial markers) and leads to less noisy reconstructions allowing a reliable and reproductive volume interpretation.

The setup of STEM-HAADF tomography is becoming more user friendly with the new suites of software for the handling of the microscope as well as for the steps of calibration of acquisition parameters and focusing. STEM images suppose that all the points of the sample are placed at the same focal plane during the scanning. This condition does not occur during tomographic acquisition due to sample tilting, which implies a significant focus difference between the upper and the lower region of the specimen in the perpendicular direction to the tilt axis. These focus variations should be dynamically corrected, line by line, by the acquisition software [21]. The dynamic correction of focus, area by area, results in STEM-HAADF tomographic tilt series in which all the points in all the images have been acquired in focus. This, together with SNR improvement, leads to final reconstructions in which the stained biological objects are more contrasted in STEM-HAADF tomography than in standard TET, as they appears as white objects against an uniform dark background (Figure 1C,D). Therefore, the reconstructed volumes are suitable for objective segmentation methods such as thresholding [22] which, instead of relying on the subjective manual tracing of contour lines, are based in the assignation of colors or grey levels as function of the voxel values (**Figure 2**).

EFTEM tomography

Fonsecaea pedrosoi cells from 5-day old cultures were filtered in a 40–60G porous plate filter followed by centrifugation (13,600g, 30 min, 4°C) to isolate the conidial forms. Fungal conidia were fixed with 2.5% glutaraldehyde in PBS, exhaustively rinsed with PBS, and incubated in the presence of 10 μg/mL cationized ferritin, at pH 7.2, for 1 h at room temperature. Cells were postfixed for 30 min in 1% osmium tetroxide, dehydrated in acetone, and embedded in Epon [23]. 150 nm thick sections were used for observations under the electron microscope by TET and in EFTET.

The main advantage of EFTET is that it complements the structural information obtained by standard TET by providing the 3D localization of studied chemical elements. Therefore the process today is almost fully automatized, one drawback in

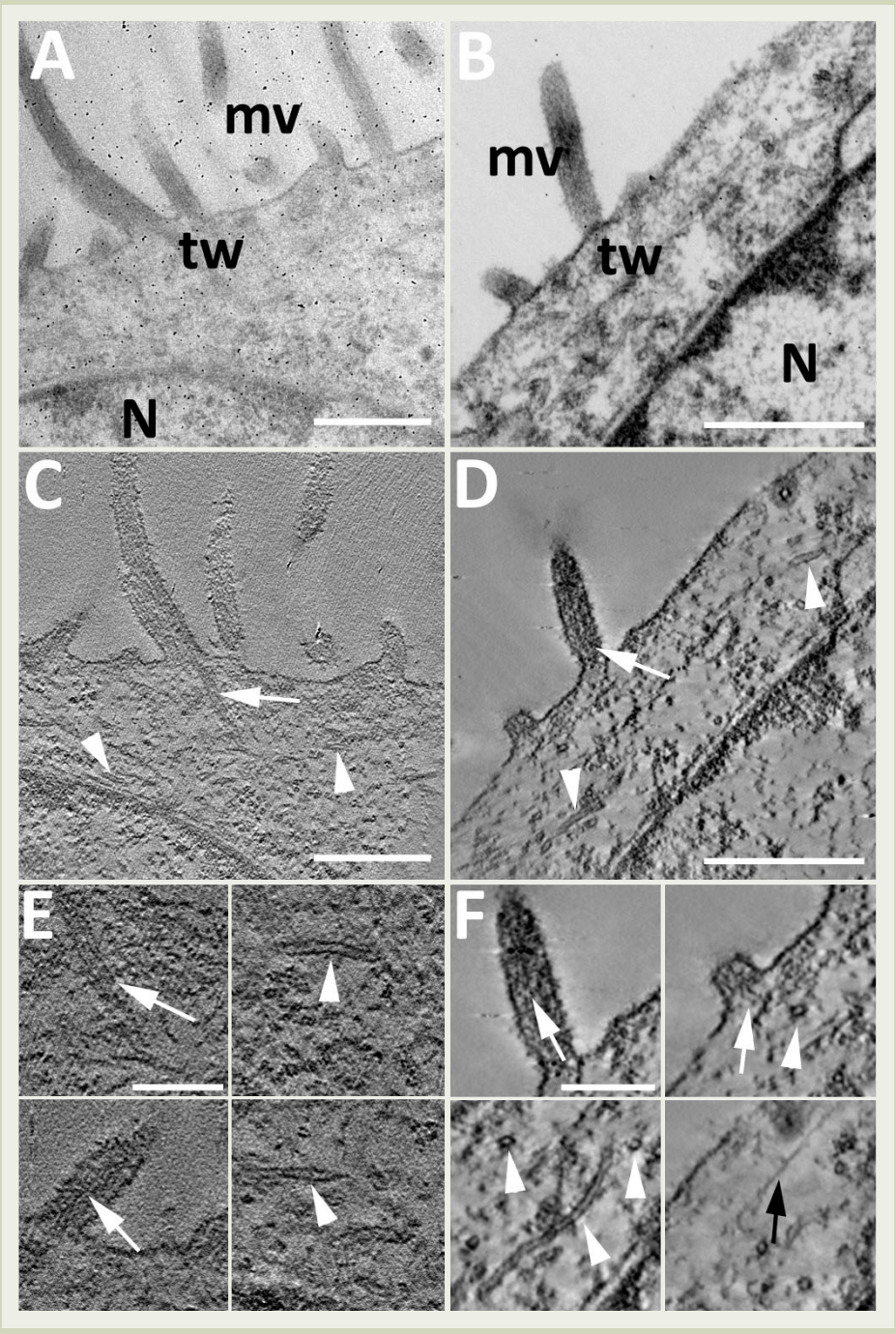

Fig. 1 **Comparison between TET and STEM-HAADF tomography.** A) 0° tilt image TEM; B) 0° tilt image STEM in a similar region of the same sample from the cell shown in (A). C) Virtual section extracted from TET tomogram computed from tilt series corresponding to (A). D) Virtual section extracted from STEM-HAADF tomogram computed from the tilt series corresponding to (B). E) Virtual cropped sections of areas of interest from (A). F) Virtual cropped sections of areas of interest from (B). N=nucleus, tw= terminal web, mv=microvilli. White arrow=actin filament; white arrowhead=microtubules; black arrows=intermediate filaments. Scale bars: A-D 500 nm, E-F 200 nm.

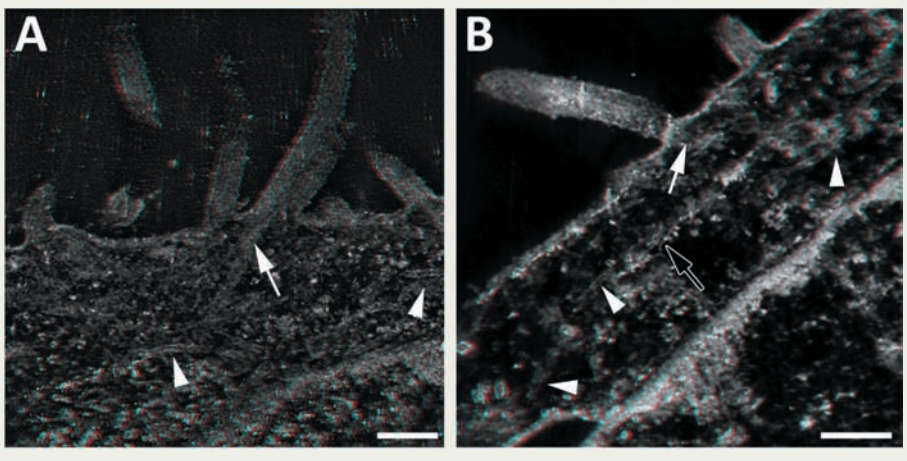

Fig. 2 **Anaglyph from threshold segmentation TET and STET.** White arrow=actin filament; white arrowhead=microtubules; black arrows=intermediate filaments. Scale bars 200 nm. Require red-cyan anaglyph glasses.

EFTET is that acquisition is time consuming due to the need of a high number of images to be acquired at different energy loss values for each tilt angle (**Figure 3**). In addition, this may result in a high electron dose incident on the sample. Objects too sensitive to radiation might not be ideal for EFTET studies, although working at liquid nitrogen or lower temperature may reduce the negative effects of the radiation damage [24]. In the case of EFTET, one important procedure is computation of the reconstruction, since image alignment must be very precise, what can be increasingly difficult due to the low signal-to-noise ratio frequently occurring in data from biological samples. An additional improvement to achieve a good EFTEM tomogram is associated to the prerequisite of unspecific background subtraction which should be based on robust algorithms because it can lead to the overestimation of characteristic signal of the studied element. The use of different law models for background subtraction and of multivariate statistical analysis (MVA) can prevent for this overestimation allowing the computation of accurate maps [25]. Despite these obstacles for the inexperienced user, EFTET should be encouraged since it allows the study of the distribution of specific chemical elements in the sample volume, and its use become justified to prevent incorrect interpretations only based on contrast. Once 3D chemical maps are correctly computed, the returned information gives access to precise elemental positioning in a sample [26].

In our samples, as the TEM image shown in Figure 3, different dark particles can be observed associated to the fungal cell wall. These particles are usually interpreted as ferritin aggregates which are associated with melanin pigments. However, the computation of the 3D electron map after the use of MVA (**Figure 4**) demonstrates that not every electron dense area correspond to iron. This map was validated by the quantification of the signal measured at different regions of the sample.

Conclusions

This study has shown that STEM-HAADF tomography is suitable and should be encourage for the study of small, low contrasted, resin embedded biological samples since provide an improvement of the SNR on reconstructed volumes. This results in the observation of delimited borders against a near-homogenous background on the 3D reconstructions, facilitating the interpretation of the images or allowing them to be used for automatic or semi-automatic segmentation. Regarding EFTEM tomography, it adds the important information of the 3D localization of defined chemical elements which complements the structural data obtained by standard TET. Both, STEM-HAADF and EFTEM tomographies are techniques that will be more applied in future researches in cell biology and microbiology and they are also an important basis for approaches that are currently in development which allow the specific labeling of proteins, by specific heavy metal associated clonable tags [27].

Acknowledgements

Authors want to thanks Dr. Monique Arpin from the Institut Curie in Paris (France) for providing LLC-PK1 cells. Dr. Sonia Rozental from the Universidade Federal do Rio de Janeiro (Brazil) for the kind donation of fungal samples. The "Fondation pour la Recherche Médicale" for the fellowship of MC, and "Region Ile de France" for its contribution on the purchase of the JEOL JEM-2200FS microscope used for every experiment reported in this manuscript.

References

[1] Seeram E., Computed Tomography: Physical Principles, Clinical Applications, and Quality Control (CONTEMPORARY IMAGING TECHNIQUES), 3rd edition, Sauders Elsevier, (2008).

[2] Wernick M.N. and Aarsvold J.N., Emission Tomography: The Fundamentals of PET and SPECT, Elsevier Academic Press, (2004).

[3] Liang Z. & Laut erbur P.C., Lauterbur., Principles of Magnetic Resonance Imaging: A Signal Processing Perspective, IEEE Press Sereies in biomedical Engineering, (2000).

[4] Christian P. E. Christian & Kristen M. Waterstram-Rich, Nuclear Medicine and PET/CT Technology and Techniques, Springer, (2007).

[5] Bárcena M. Koster A.J. Electron tomography in life science. *Semin Cell*

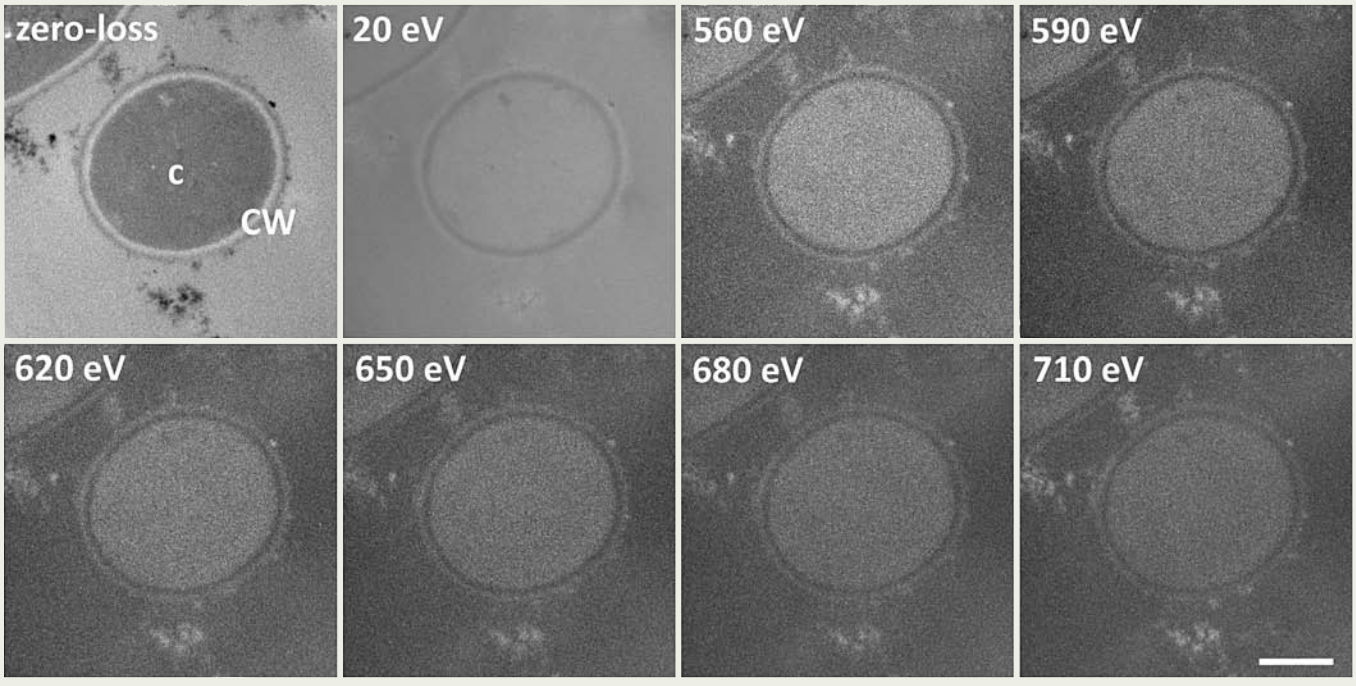

Fig. 3 **Untilted images extracted from *F. pedrosoi* tomographic series.** A) 0° tilt-images recorded at different energies values between 0 and 710 eV. C= cytoplasm, CW= cell wall. Scale bars 400 nm.

Dev Biol. **20**(8), 920-930 (2009).
[6] Herman, G.T., Fundamentals of computerized tomography: Image reconstruction from projection, 2nd edition, Springer, (2009).
[7] Larabell C.A. Nugent K.A. Imaging cellular architecture with X-rays. *Curr Opin Struct Biol*. **20**(5), 623-31 (2010).
[8] Frank J., Electron Tomography: Methods for Three-Dimensional Visualization of Structures in the Cell, Springer, (2006).
[9] Vanhecke D., Graber W. Studer D. Close-to-native ultrastructural preservation by high pressure freezing. *Methods Cell Biol*. **88**, 151-64 (2008).
[10] Dubochet J., Adrian M., Chang J. J., Homo J. C., Lepault J. McDowall A. W., Schultz P. Cryo-electron microscopy of vitrified specimens. *Q Rev Biophys*. **21**(2), 129-228 (1988).
[11] Mader A., Elad N. and Medalia O. Cryoelectron tomography of eukaryotic cells. *Methods Enzymol*. **483**, 245-65 (2010).
[12] Friedrich H., McCartney M.R. Buseck P.R. Comparison of intensity distributions in tomograms from BF TEM, ADF STEM, HAADF STEM, and calculated tilt series. *Ultramicroscopy* **106**(1), 18-27 (2005).
[13] Midgley P.A. Weyland M. 3D electron microscopy in the physical sciences: the development of Z-contrast and EFTEM tomography. *Ultramicroscopy* **96**(3-4), 413-31 (2003).
[14] Frixione E. Recurring views on the structure and function of the cytoskeleton: a 300-year epic. *Cell Motil Cytoskeleton*. **46**(2), 73-94 (2000).
[15] Ikeda R., Sugita T., Jacobson E.S. Shinoda T. Effects of melanin upon susceptibility of *Cryptococcus* to antifungals. *Microbiol Immunol*. **47**(4), 271-277 (2003).
[16] Franzen A.J., Cunha M.M., Miranda K., Hentschel J., Plattner H., da Silva M.B., Salgado C.G., de Souza W. Rozental S. Ultrastructural characterization of melanosomes of the human pathogenic fungus *Fonsecaea pedrosoi*. *J Struct Biol*. **162**(1), 75-84 (2008).
[17] Kremer J.R., Mastronarde D.N., McIntosh J.R. Computer visualization of three-dimensional image data using IMOD. *J Struct Biol*. **116**(1), 71-6 (1996).
[18] http://bio3d.colorado.edu/imod/
[19] Messaoudi C., Boudier T., Sanchez Sorzano C.O. and Marco S. TomoJ: tomography software for three-dimensional reconstruction in transmission electron microscopy. *BMC Bioinformatics*. **8**, 288 (2007).
[20] http://u759.curie.u-psud.fr/software-su759.html
[21] Biskupek J., Leschner J., Walther P. and Kaiser U. Optimization of STEM tomography acquisition - a comparison of convergent beam and parallel beam STEM tomography. *Ultramicroscopy* **110**(9), 1231-1237 (2010).
[22] Sezgin M. and Sankur B. Survey over image thresholding techniques and quantitative performance evaluation, *Journal of Electronic Imaging*. **13**(1), 146–165 (2004).
[23] Cunha M.M., Franzen A.J., Alviano D.S., Zanardi E., Alviano C.S., De Souza W. and Rozental S. Inhibition of melanin synthesis pathway by tricyclazole increases susceptibility of *Fonsecaea pedrosoi* against mouse macrophages. *Microsc Res Tech*. 15, **68**(6), 377-84 (2005).
[24] Aronova M.A., Sousa A.A., Zhang G. and Leapman R.D.. Limitations of beam damage in electron spectroscopic tomography of embedded cells. *J Microsc*. **239**(3), 223-232 (2010).
[25] Quintana C., Marco S., Bonnet N., Risco C., Gutiérrez M.L., Guerrero A. and Carrascosa J.L.. Optimization of phosphorus localization by EFTEM of nucleic acid containing structures. *Micron*. **29**(4), 297-307 (1998).
[26] Weyland M., Yatesa T.J.V., Dunin-Borkowskia R.E., Laffonta L. and Midgley P.A., Nanoscale analysis of three-dimensional structures by electron tomography. *Scripta Materialia*, **55**(1), 29-33 (2006).
[27] Mercogliano C.P. DeRosier D.J.. Concatenated metallothionein as a clonable gold label for electron microscopy. *J Struct Biol*. **160**(1), 70-82 (2007).

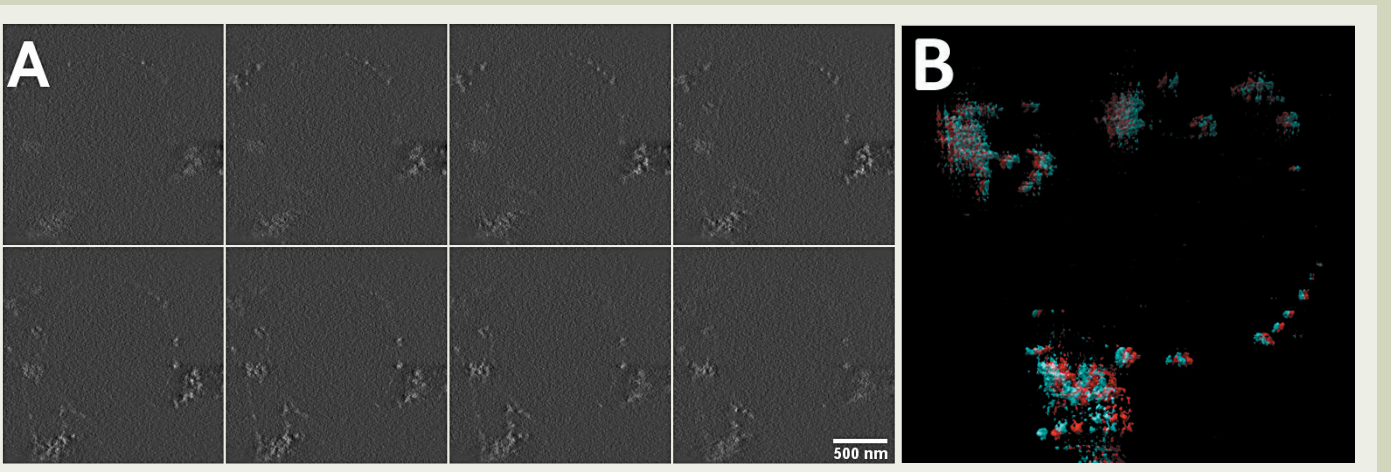

Fig. 4 **Iron localization in *F. pedrosoi* by EFTEM tomography after addition of ferritin for melanin detection.** A) Sections of the reconstructed iron map after MVA filtering extracted each 16 nm. Scale bar 500 nm. B) Anaglyph of threshold based segmented iron map. Require red-cyan anaglyph glasses.